Re--direction of interferon gamma and its signaling moiety

Bansal, Ruchi

IMPORTANT NOTE: You are advised to consult the publisher's version (publisher's PDF) if you wish to cite from it. Please check the document version below.

Document Version
Publisher's PDF, also known as Version of record

Publication date:
2012

[Link to publication in University of Groningen/UMCG research database](#)

Citation for published version (APA):
Bansal, R. (2012). *Re--direction of interferon gamma and its signaling moiety: new options for the therapy of chronic diseases*. s.n.

Chapter 2

PEGylation Improves Pharmacokinetic Profile, Liver Uptake and Efficacy of Interferon Gamma in Liver Fibrosis

Ruchi Bansal, Eduard Post, Johannes H. Proost, Alie de Jager-Krikken, Klaas Poelstra, Jai Prakash

ABSTRACT

Interferon gamma (IFNγ) is a potent cytokine that displays a variety of anti-viral, anti-proliferative, immunomodulatory, apoptotic and anti-fibrotic functions. However, its clinical use is limited to the treatment of few diseases due to the rapid clearance from the body. PEGylated IFN-alpha formulations are shown to be beneficial in viral hepatitis, but PEGylation of IFNγ to enhance its therapeutic effects in liver fibrosis is not yet explored. Liver fibrosis is characterized by the extensive accumulation of an abnormal extracellular matrix and is the major cause of liver-related morbidity and mortality worldwide. To date,
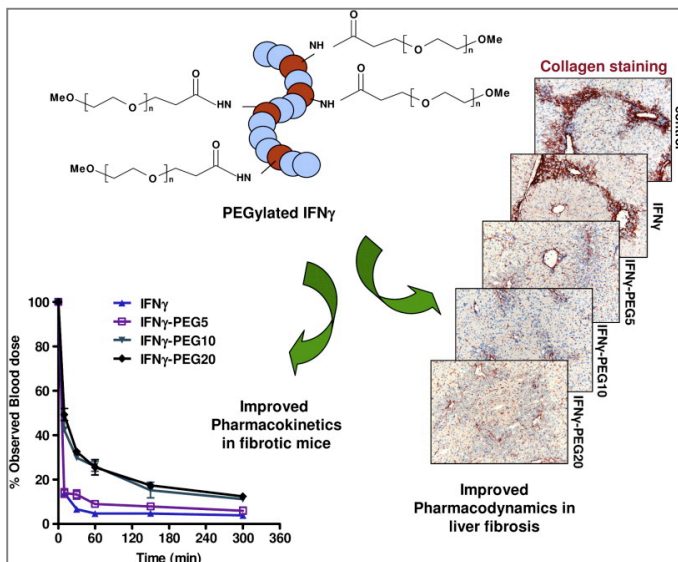
there is no pharmacotherapy available for this disease. We modified IFNγ with different-sized linear PEG molecules (5, 10 and 20 KDa) and assessed the biological activity *in vitro* and *in vivo*. All PEGylated IFNγ constructs were biologically active and activated IFNγ signaling *in vitro* as determined with a nitric oxide release assay and a pGAS-Luc reporter plasmid assay, respectively. Similar to IFNγ, all PEGylated IFNγ induced a significant reduction of fibrotic parameters in mouse NIH3T3 fibroblasts as shown with immunohistochemical staining and quantitative PCR analyses. *In vivo*, the pharmacokinetic profile of radiolabeled ^{125}I-IFNγ-PEG conjugates revealed a decreased renal clearance and an increased plasma half-life with an increase of PEG size. Moreover, the liver accumulation of PEGylated IFNγ constructs was significantly higher than the unmodified IFNγ, which was also confirmed by increased MHC-II expression in the livers. Furthermore, in a CCl_4-induced acute liver injury model in mice, PEGylated constructs reduced the early fibrotic parameters more drastically than unmodified IFNγ. Of note, these effects were stronger with higher PEG-sized IFNγ constructs. These data nicely correlated with the pharmacokinetic data. In conclusion, PEGylation significantly improved the pharmacokinetics, liver uptake and anti-fibrotic effects of IFNγ. This study opens new opportunities to exploit the therapeutic applications of PEGylated IFNγ for the treatment of liver fibrosis and other diseases.

1. INTRODUCTION

Liver fibrosis, mainly caused by viral hepatitis, alcohol consumption and obesity, is characterized by an excessive production of extracellular matrix proteins that form hepatic scars. If untreated, this leads to cirrhosis and eventually hepatocellular carcinoma [1,2]. Following liver injury, growth factors and cytokines, produced due to hepatocyte damage, lead to the activation of hepatic stellate cells (HSC). HSC subsequently transdifferentiate into proliferative, contractile and extracellular matrix producing myofibroblasts [3,4]. Despite evolving experimental therapies for liver fibrosis in animals, to date none has been clinically approved, leaving liver transplantation as the only therapeutic option [5]. Treatment of hepatitis B and C infections has been quite successful in recent years mainly due to the development of PEGylated IFNα molecules that have an optimal pharmacokinetic profile combined with potent antiviral activity. This illustrates the potential of using endogenous cytokines for therapeutic purposes. Interferon gamma (IFNγ) has been shown to display potent anti-fibrotic effects *in vitro* and in animal models [5,6], therefore we examined whether modified forms of IFNγ can be used as anti-fibrotic drugs.

During liver injury, IFNγ is produced by inflammatory cells as a self-defensive mechanism. In rodents, disruption of IFNγ or its signaling via signal transducer and activator of transcription (STAT1) enhanced liver fibrosis while treatment with IFNγ ameliorated hepatic fibrosis induced by CCl_4 and dimethylnitrosamine (DMN) [13,14]. But its reduced bioavailability due to poor pharmacokinetics reduces its potency. Although a number of approaches have been developed to increase the half-life of cytokines or other protein drugs, fewer attempts have been made for IFNγ [15]. PEGylation, the covalent attachment of polyethylene glycol (PEG), has modified a variety of therapeutic drugs into an effective and potent compounds compared to their unmodified parent molecules. This is one of the common approaches used to improve the pharmacokinetics, immunological and pharmacodynamics properties of therapeutic proteins [16-19]. PEGylated formulations of IFNα (PEGIntron and PEGASYS) are exemplar clinically approved drugs for the treatment of hepatitis C [20,21]. Surprisingly, knowing the potential of IFNγ, PEGylation of IFNγ has not been reported.

In the present study, we synthesized different PEGylated formulations of IFNγ using different sized PEG molecules and evaluated their biological activity *in vitro*. Subsequently, we examined their pharmacokinetics and investigated *in vivo* therapeutic efficacy in a CCl_4-induced acute liver fibrosis model in mice. To our best knowledge, this is the first comprehensive study presenting the pharmacokinetics and efficacy of different PEGylated IFNγ formulations in liver fibrosis.

2. MATERIALS AND METHODS

2.1. Synthesis and characterization of PEGylated IFNγ conjugates

Murine IFNγ (0.32nmol, 50μg/ml dissolved in PBS; Peprotech, London, UK) was reacted with 16nmol of different sized PEG succinimidyl ester (6.4μl of 12.5mg/ml mPEG-

NHS5, 25mg/ml mPEG-NHS10 and 50mg/ml mPEG-NHS20 dissolved in PBS). mPEG-NHS of different sizes (5KDa, 10KDa and 20KDa) were purchased from Creative PEG works, Winston Salem, NC. The reaction was performed at 4°C for overnight on a slow vortex. The synthesized products were extensively dialyzed against PBS using suitable dialysis membranes. For purification of IFNγ-PEG5 and IFNγ-PEG10, 10KDa cut-off low protein binding dispodialyzers were used and for purification of IFNγ-PEG20, 25KDa cut-off low protein binding dispodialyzers (Harvard Apparatus, Holliston, Massachusetts) were used. Similar steps were followed with unmodified IFNγ, where 0.32nmol murine IFNγ (50µg/ml dissolved in PBS) was mixed with 6.4µl of PBS, incubated overnight and dialyzed against PBS using 10KDa cut-off dispodialyzers. Since the protein concentrations used for the reactions were too low (5µg) to detect with quantitative assays, final concentrations were calculated based on the initial amounts added to the reaction mixtures. All the steps were kept similar for free and PEGylated IFNγ and equivalent protein concentrations were used further in *in vitro* and *in vivo* experiments.

The IFNγ conjugates were characterized by SDS-PAGE analysis followed by barium-iodide PEG staining. Briefly, 25µl of IFNγ conjugates (equivalent to 250ng) were subjected to SDS-PAGE (10%) according to standard protocols. After running the gel, PEGylated IFNγ formulations were detected with PEG staining as follows. The gels were rinsed with water, followed by fixation in perchloric acid (0.1M) for 15 min. The gels were washed again and treated with barium chloride (5%) for 10min. Subsequently the color was developed using tritisol Iodine solution (Sigma, St. Louis, MO). The gels were photographed using G-Box (Syngene, Cambridge, UK). In addition to PEG staining, western blotting was performed where the SDS-PAGE gel was run with 100ng of protein. The separated proteins were then transferred to PVDF membrane and the membranes were blocked with TBST (20mM TrisHCl, pH 7.6, 154mM NaCl, 0.1% Tween 20) containing 5% skimmed milk. The blots were incubated with either rabbit polyclonal IFNγ antibody (Abcam, Cambridge, UK) for 1h at room temperature. After three washings with TBST, the blots were incubated with HRP-conjugated goat anti-rabbit antibody (DAKO, Glostrup, Denmark) for 1h and were developed using western lightning-ECL reagent (Perkin-Elmer, Boston, MA) according to the manufacturer's instructions.

2.2. Cell lines

Mouse NIH3T3 fibroblasts and mouse RAW macrophages were obtained from American type culture collection (ATCC, Rockville, MD). NIH3T3 fibroblasts and RAW macrophages were cultured in Dulbecco's modified Eagle's medium (DMEM, Invitrogen, Carlsbad, CA) supplemented with 10% FBS (Invitrogen) and antibiotics (50U/ml penicillin plus 50ng/ml streptomycin). After attaining 80% confluency (3-4 days), cells were passaged and $1x10^6$ cells were plated in fresh T75 flask. Mouse NIH3T3 fibroblasts were used from passage 160 to passage 170 and RAW macrophages were used between passage 13 and passage 19.

2.3. In vitro experiments

2.3.1 Nitric oxide (NO) release bioassay in mouse RAW macrophages

The bioactivity of IFNγ and IFNγ conjugates was assessed by measuring the accumulation of nitrite NO_2, a stable nitric oxide (NO) metabolite produced by RAW macrophages as previously described [22]. Briefly, cells ($1x10^5$cells/200µl/well) were seeded in 96-well plates and grown overnight at 37°C/5% CO_2. Then either medium alone, IFNγ or PEGylated IFNγ conjugates were added at different concentrations (5, 10, 25 and 50 ng/ml diluted from 1µg/ml stock solutions) with or without 100ng/ml lipopolysaccharides (LPS from E.coli 055:B5, Cat. no. L-6529, Sigma) prepared from 1mg/ml stock. After 24h, the secreted nitrite was measured using Griess reagent (1% sulfanilamide; 0.1% naphthylethylendiamine dihydrochloride; 3% H_3PO_4). The absorbance was determined at 550nm using an ELISA plate reader.

2.3.2 Plasmid transfection assay in NIH3T3 fibroblasts

The signaling pathway of IFNγ and PEGylated IFNγ constructs was determined with a Luciferase assay using a Luciferase containing cis-reporter plasmid DNA, pGAS-Luc (Stratagene, La Jolla, CA), which contains four direct repeats of the IFN gamma-activating sequence (GAS) upstream of the TATA box and a luciferase gene. pCIS-CK was used as a control plasmid that contains luciferase reporter gene but lacks a GAS enhancer sequence. 1×10^4 cells per well were seeded in 96-well plates, and the plasmid transfection was performed after 24h using FuGENE-6 Transfection Reagent (Roche Diagnostics, Mannheim, Germany). Cells were treated with 0.17µg DNA/0.5µl FuGENE-6 complex in 100µl of normal medium with 10% FCS for 24h. Subsequently, cells were washed with serum-free medium and incubated with different concentrations (5, 25, 100, 200 and 500 ng/ml diluted from 1µg/ml stock solutions) of IFNγ or PEGylated IFNγ for 6h. Thereafter, cells were washed with PBS and lysed using 20µl of lysis buffer and subsequently 100µl of luciferase substrate (Promega, Madison, WI) was added. Luciferase activity was measured by a luminometer (Lumicount; Packard, Meriden, CT) and the luminescence unit values of pGAS-Luc were neutralized by subtracting from that of pCIS-CK values.

2.3.3 Anti-fibrotic effects of PEGylated IFNγ conjugates in NIH3T3 fibroblasts

NIH3T3 cells were seeded in 24-well culture plates (3×10^4 cells per well) or 12-well plates (1×10^5 cells/well) and grown overnight. The cells were then washed twice with PBS and starved for 24h in serum-free medium. Subsequently, cells were incubated with IFNγ or PEGylated IFNγ (equivalent 1µg/ml IFNγ prepared from 25µg/ml stock) alongwith 5ng/ml of recombinant human transforming growth factor-beta (TGFβ, diluted from 1µg/ml stock, Roche Diagnostics) for 24h. Thereafter, cells were fixed and immunostained for collagen type I/III and α-SMA as described below. In addition, cells were lysed with lysis buffer constituted with β-mercaptoethanol (Stratagene) to perform quantitative PCR analysis for procollagen 1α1, α-SMA and GAPDH (house-keeping gene) as described below.

2.4. Pharmacokinetics of radiolabeled IFNγ and PEGylated IFNγ constructs

IFNγ and IFNγ-PEG constructs were radiolabeled with ^{125}I radiolabel using N-bromosuccinimide. Briefly, an equal volume of HCl was added to the sodium salt of ^{125}I for

neutralization and then 50µl Tris/HCl buffer (1M) was added. Subsequently, N-bromosuccinimide (3.2nmol) was added to IFNγ and the IFNγ-PEG constructs (0.32nmol) followed by vortex for 30s. Labeled compounds were then purified extensively using 7KDa zeba spin desalting columns (Thermo scientific Rockford, IL) to receive > 95% purity. Mice were intravenously injected with tracer doses (5 x 10^5 cpm equivalent to 150ng/mice) of ^{125}I-IFNγ, ^{125}I-IFNγ-PEG5, ^{125}I-IFNγ-PEG10 and ^{125}I-IFNγ-PEG20. At indicated time points after administration (10, 30, 60, 150 and 300 min), the animals were sacrificed and blood samples were collected by heart puncture. The organs were excised, washed in saline and weighed after which the ^{125}I-radioactivity was counted with a γ-counter. Plasma was prepared by centrifugation of blood at 2000g for 20 min. The total radioactivity per organ was calculated and corrected for blood-derived radioactivity using correction factors. This correction factor was calculated from bio-distribution studies with albumin, which remains in the circulation during the time frame of this experiment. Pharmacokinetic (PK) analysis was performed using the Multifit program (Department of Pharmacokinetics, Toxicology and Targeting, University of Groningen, The Netherlands). The plasma concentration curves were fitted from 0 to 300 min with the Marquardt algorithm and the constant relative error variance model (weighting). An Iterative two-Stage Bayesian population analysis was applied to obtain the population pharmacokinetic parameters using a separate analysis for different groups. This analysis results in estimates for the mean and standard deviation of each parameter. Initial estimates were obtained from a standard two-stage analysis. It was demonstrated that the final population pharmacokinetic parameters were independent of initial estimates. Moreover, the data were fitted to a one and a two-compartment model. The goodness of fit was assessed by the Akaike Information Criterion (AIC). The goodness of fit was best for the two-compartment model. The pharmacokinetic parameters calculated from the proposed model:

$AUC_{(0-\infty)}$ *area under the curve from zero to infinity*

Vss = V1+V2 (V1 and V2 are the parameters derived from population PK analysis)

CL (total plasma clearance) = Dose/$AUC_{(0-\infty)}$

2.5. CCl$_4$-induced acute liver fibrosis model in mice

Normal male balb/c mice (20-22 g) were obtained from Harlan (Zeist, The Netherlands). The animals were kept in cages and received *ad libitum* normal diet, at a 12 h light and 12 h dark cycle. All experimental protocols for animal studies were approved by the Animal Ethics Committee of the University of Groningen. Acute liver injury was induced in male C57BL/6 mice by a single intra-peritoneal injection of 1 ml/kg CCl$_4$ (1:5 dilution in olive oil) at day one [23,24]. At day 2 and day 3, mice intravenously received IFNγ, IFNγ-PEG5, IFNγ-PEG10, IFNγ-PEG20 (equivalent to 5 µg IFNγ/mouse/day) or PBS alone. At day 4, all mice were sacrificed; blood and different organs were collected for further analysis.

2.6. Immunohistochemistry and immunofluorescence

The cells were fixed with acetone:methanol (1:1), dried and stored until immunostaining. Livers were harvested and transferred to Tissue-Tek OCT embedding medium (Sakura Finetek, Torrance, CA), and snap-frozen in isopentane chilled in a dry ice. Cryosections (4µm) were cut using a Leica CM 3050 cryostat (Leica Microsystems, Nussloch, Germany). The sections were allowed to adhere to Superfrost microscopic glass slides (Menzel-Gläser, Braunschweig, Germany), air-dried and fixed with acetone for 10 min. Cells or tissue sections were rehydrated with PBS and incubated with the primary antibody in appropriate dilution (refer to **supplementary table 1**) for 1h at room temperature. Cells or sections were incubated with horseradish peroxidase (HRP)-conjugated secondary antibody for 30 min at room temperature. Then, cells or sections were washed with 1x PBS for 15 min (5 min each). Following incubation with HRP-conjugated tertiary antibody for 30 min after which cells or sections were washed thrice with 1x PBS. Thereafter, peroxidase activity was developed with 3-amino-9-ethyl carbazole (Sigma, St. Louis, MO) for 20 min and nuclei were counterstained with hematoxylin (Fluka Chemie, Buchs, Switzerland). Cells or sections were mounted with Kaiser's gelatin (Darmstadt, Germany) and visualized using a light microscope (Olympus UK Ltd., Essex, UK). α-SMA staining was performed using M.O.M kit (vector laboratories, Burlingame, CA) according to the manufacturer's instructions. For quantitation, 27 microscopic fields at 200x magnification per liver section from each mouse were captured. The stained area in the digital photomicrographs was quantified using automated Cell-D imaging software (Olympus) according to standard procedures.

2.7. Quantitative real time PCR

Total RNA from cells and liver tissues was isolated using absolutely RNA microprep kit (Stratagene) and RNeasy mini kit respectively (Qiagen, Hilden, Germany) according to manufacturer's instructions. The RNA concentration was quantitated by a UV spectrophotometer (NanoDrop Technologies, Wilmington, DE). Total RNA (1.6µg) was reverse transcribed in a volume of 50µl using cDNA synthesis kit (Promega). All the primers were purchased from Sigma-Genosys (Haverhill, UK). The sequences of primers used in the study are enlisted in **supplementary table 2**. 20ng of cDNA was used for quantitative real time PCR analysis. The reactions were performed using SYBR green PCR master mix (Applied Biosystems) according to the manufacturer's instructions and were analyzed by ABI7900HT sequence detection system (Applied Biosystems). Finally, the threshold cycles (Ct) were calculated and relative gene expression was normalized with GAPDH (for mouse) and 18srRNA (for human) as housekeeping genes.

2.8. Statistical analyses

Data are presented as mean ± standard error of the mean (SEM). Multiple comparisons between different groups were performed by one-way analysis of variance (ANOVA) with Bonferroni post-test.

3. RESULTS

3.1. Syntheses and characterization of PEGylated IFNγ conjugates

IFNγ was directly conjugated to different sized polyethylene glycol molecules (PEG 5, 10, 20 KDa) as depicted in a schematic representation in **Figure 1A.** The successful PEGylation of IFNγ was confirmed by SDS-PAGE analysis followed by barium-iodide staining for PEG molecules and western blot analysis using anti-IFNγ antibody. **Figure 1B**
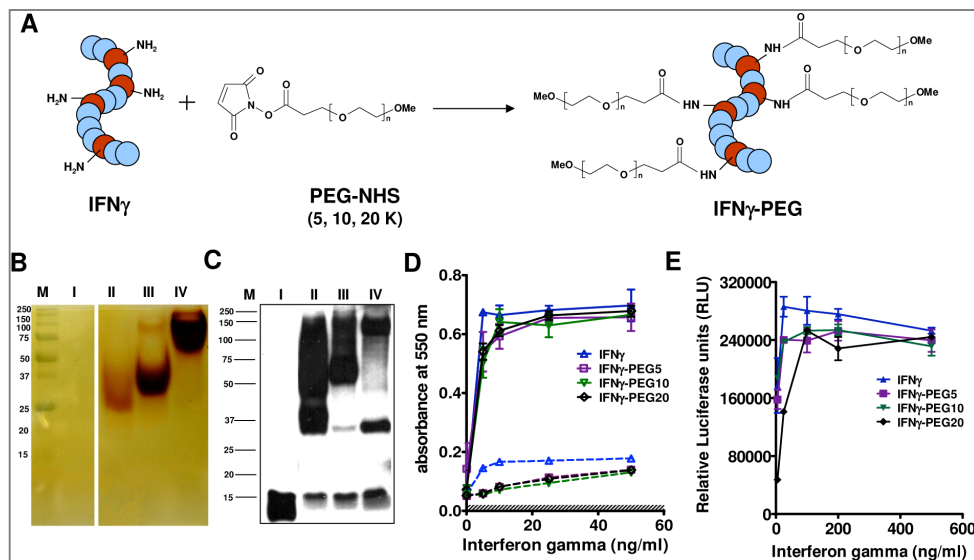
**Figure 1: Synthesis and *in vitro* functional characterization of PEGylated IFNγ constructs. (A)** Schematic synthesis of PEGylated IFNγ. **(B)** PEG staining illustrates the successful synthesis of PEGylated IFNγ conjugates. **M** denotes molecular weight markers in KDa; Lane I: unmodified IFNγ, Lane II: IFNγ-PEG5 conjugate; Lane III: IFNγ-PEG10 conjugate; Lane IV: IFNγ-PEG20 conjugate. The shift in the bands indicates successful PEG coupling of approx. 2-3 PEG moieties per IFNγ molecule. **(C)** Western blot analysis using anti-IFNγ antibody showing formation of PEGylated IFNγ adducts and presence of ≤ 10% free IFNγ. **M** denotes molecular weight markers in KDa; Lane I: unmodified IFNγ, Lane II: IFNγ-PEG5 conjugate; Lane III: IFNγ-PEG10 conjugate; Lane IV: IFNγ-PEG20 conjugate. **(D)** Nitrogen oxide (NOx) release in mouse RAW macrophages (n=3) after incubation with unmodified IFNγ and IFNγ-conjugates in absence of LPS (denoted by open symbols) and presence of LPS (denoted by closed symbols). Shaded area denotes response to LPS alone without IFNγ. **(E)** Relative Luciferase expression measured to assess the signaling pathway of IFNγ and PEGylated-IFNγ constructs using a Luciferase containing cis-reporter plasmid DNA, pGAS-Luc. Data represent three independent experiments performed in triplicates.

and **Figure 1C** show the shift in protein bands after PEGylation. The shifts indicated the successful coupling of PEG molecules to IFNγ molecule as determined with molecular weight ladder. Western blot analysis showed formation of multiple PEGylated adducts of IFNγ during the conjugation reactions and indicated the presence of ≤10% unconjugated free IFNγ (**Figure 1C, supplementary Table 3**).

3.2. In vitro biological effects of PEGylated IFNγ conjugates

Since chemical modification can affect the biological activity of IFNγ, we examined the bioactivity of PEGylated IFNγ conjugates versus unmodified IFNγ in mouse RAW macrophages using a standard nitric oxide (NO) release assay. IFNγ and PEGylated IFNγ constructs caused a dose-dependent increase in NO production in the absence and presence of LPS (**Figure 1D**). PEGylated IFNγ constructs induced a reduction in NO production as compared to free IFNγ in absence of LPS while there was no significant difference in the dose response curves of PEGylated IFNγ constructs compared to unmodified IFNγ in presence of LPS (**Figure 1D**). PEGylation might also hinder the interaction of IFNγ with its receptor thereby influencing the IFNγ signaling pathway. IFNγ-IFNγR interaction results in the activation of the JAK-STAT pathway and activates signal transducers and activators of transcription (STAT1) that binds to unique gamma-activated sequence (GAS) regulating IFNγ-responsive genes [25,26].
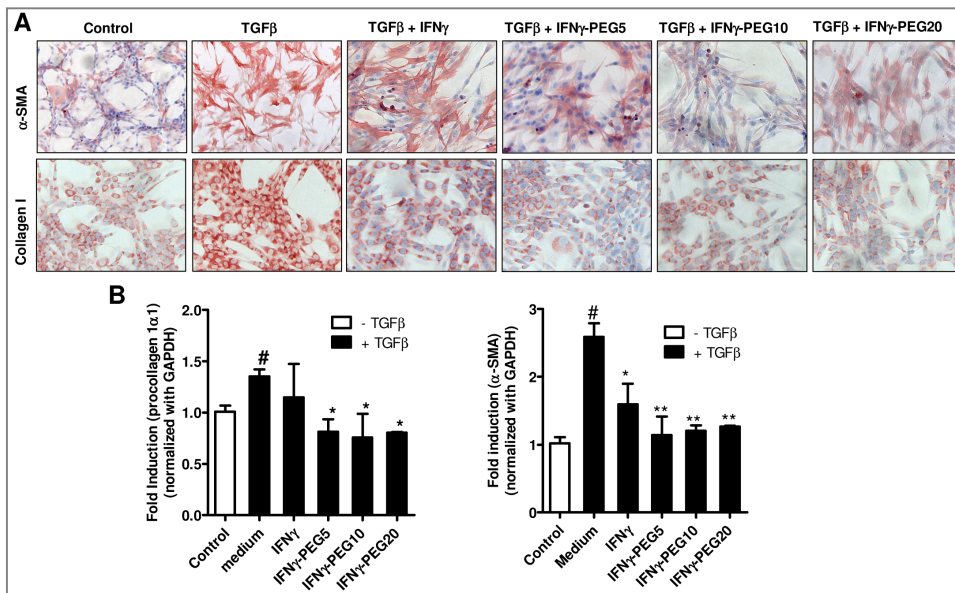
**Figure 2: Reduction of fibrotic parameters with PEGylated IFNγ constructs in NIH3T3 fibroblasts. (A)** Representative pictures (n=3) of collagen I/III stained NIH3T3 cells, incubated with medium alone (control) or TGFβ (5ng/ml) in combination with IFNγ or IFNγ-conjugates (1μg/ml). (B) Effects of different constructs on the gene expression of procollagen1α1 and α-SMA. Data represent the mean ± SEM for three independent experiments.

We examined the signaling pathway induced by IFNγ-PEG constructs and unmodified IFNγ in mouse NIH3T3 fibroblasts using the pGAS-Luc cis-reporter plasmid assay where the luciferase gene is downstream of the GAS enhancer sequence. A dose-dependent increase in luciferase expression (luminescence) by both IFNγ and IFNγ-PEG constructs indicated that there were no significant differences between IFNγ and IFNγ-PEG constructs (**Figure 1E**).

Subsequently, we investigated the anti-fibrotic effects of the PEGylated constructs in mouse NIH3T3 fibroblasts after activation with TGFβ1. We found that TGFβ1–induced fibroblast activation (α-SMA expression) and collagen expression were significantly inhibited by IFNγ and more strongly with IFNγ-PEG constructs both at protein and mRNA transcript levels (**Figure 2A and B**).

3.3. Induction of IFNγ receptor expression during liver fibrosis

We compared the IFNγ receptor expression levels in fibrotic human and mouse livers versus normal livers using immunohistochemistry and mRNA analyses. PAS staining showed the liver damage in human and mice (**Figure 3A and 3C**). Both protein and mRNA analyses revealed that IFNγR was significantly upregulated in cirrhotic human livers and in acute CCl_4-induced fibrotic mouse livers (**Figure 3A-D**).
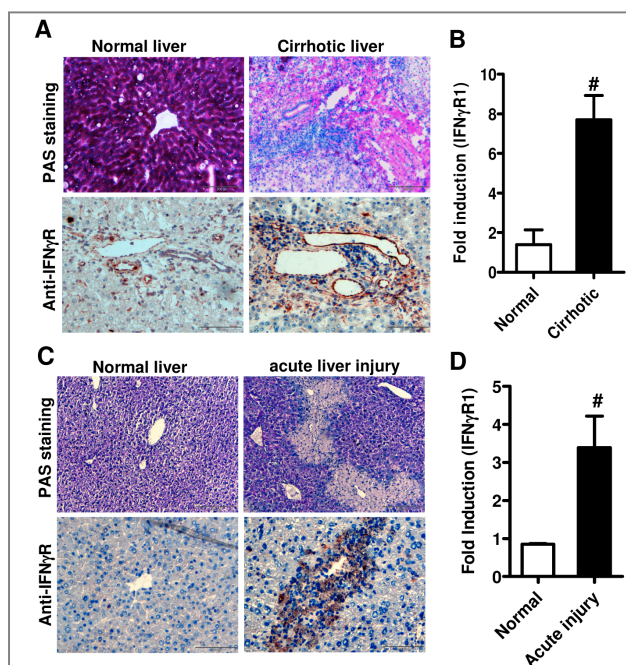

Figure 3: IFNγ receptor expression in fibrotic versus normal livers in human (A, B) and mice (C, D). Representative photomicrographs illustrating PAS staining and IFNγR expression in cirrhotic human liver **(A)** and in CCl_4-induced fibrotic mouse livers **(C)** versus respective normal livers. Scale bars; 100µm. IFNγR mRNA levels in cirrhotic human liver, n=3 **(B)** and in CCl_4-induced fibrotic mouse livers, n=6 **(D)** were higher compared to the normal livers. Bars represent mean ± SEM. Differences versus normal are presented as #$p<0.05$.

3.4. Pharmacokinetics of PEGylated IFNγ constructs in vivo

Since IFNγR was highly upregulated during liver injury, we first compared the bio-distribution of ^{125}I-IFNγ in normal versus fibrotic mice to determine if the high receptor expression enhances its liver uptake. We found that the plasma disappearance of ^{125}I-IFNγ was similar in both cases (**Supplementary Figure 1A**). However, the liver levels were significantly increased in fibrotic livers ($AUC_{(0-∞)}$, 64 %dose*h) compared to normal livers ($AUC_{(0-∞)}$, 39.2 %dose*h) (**Supplementary Figure 1B**). These data indicate that accumulation of IFNγ is dependent on the expression of IFNγR and therefore longer circulation of IFNγ might increase liver accumulation leading to improved efficacy in fibrotic mice.

Next, we examined the pharmacokinetics of ^{125}I-labeled IFNγ and PEGylated IFNγ in the acute CCl4-induced liver injury model in mice. **Figure 4A** shows the plasma levels of radiolabeled IFNγ and PEGylated IFNγ constructs at various time points after a single intravenous injection in fibrotic mice. The pharmacokinetic parameters derived from plasma disappearance curves are shown in **Table 1**. The plasma levels were significantly
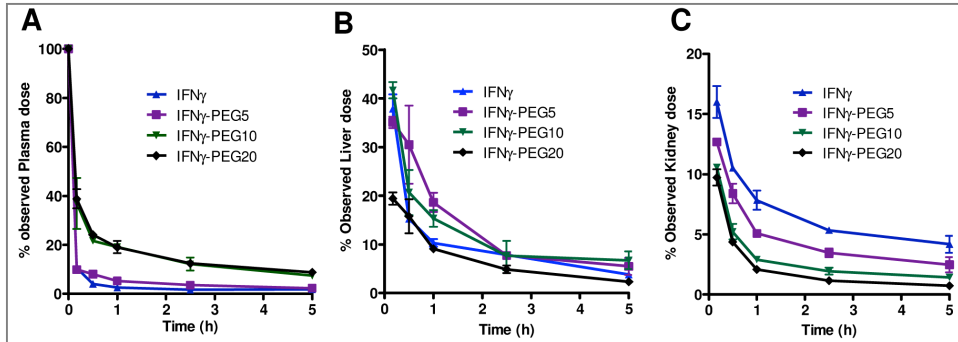
Figure 4: Pharmacokinetic profile of IFNγ versus PEGylated IFNγ in CCl4-induced acute liver injury model in mice. (A) Plasma disappearance curves of IFNγ and PEGylated-IFNγ in fibrotic mice. **(B)** Liver and **(C)** kidney accumulation at different time points after administration of radiolabeled (^{125}I)-IFNγ or (^{125}I)-PEGylated-IFNγ in fibrotic mice. n=10 mice were used per treatment group and each time point represents the mean of two animals.

increased at different time points with increasing size of PEG. The liver levels of IFNγ-PEG5 and IFNγ-PEG10 were higher after intravenous injection while administration of IFNγ-PEG20 had comparatively lower levels. This was further confirmed by calculating AUC reflecting total liver uptake (**Figure 4B** and **Table 2**). Conversely, kidney levels gradually decreased with increasing PEGylation of IFNγ (**Figure 4C** and **Table 2**).

Table 1: Pharmacokinetics parameters (two-compartment model) derived from concentration-time curves after a single intravenous dose of IFNγ and PEGylated IFNγ in fibrotic mice.

Plasma	AUC (h*%dose)	Vss (ml)	CL (ml/h)
IFNγ	27.1	18.4	3.69
IFNγ-PEG5	33.0	10.13	3.03
IFNγ-PEG10	105	3.73	0.95
IFNγ-PEG20	121	3.71	0.83

AUC(0-∞), area under the curve from zero to infinity; Vss, steady state volume of distribution; CL, Total plasma clearance.

Table 2: Liver and kidneys AUC derived from concentration-time curves after a single intravenous does of IFNγ and PEGylated IFNγ in fibrotic mice.

	Liver AUC$_{(0-\infty)}$ (h*%dose)	Kidney AUC$_{(0-\infty)}$ (h*%dose)
IFNγ	64.1	49.8
IFNγ-PEG5	78.2	30.7
IFNγ-PEG10	78.5	18.3
IFNγ-PEG20	40.2	12.0

AUC$_{(0-\infty)}$, area under the curve from zero to infinity.

We also assessed major histocompatibility class II (MHC-II) expression, which is known to be up-regulated by IFNγ [27], to assess the biological activity of the conjugates in livers. PEGylated IFNγ with increasing PEG size induced a remarkable up-regulation in MHC-II expression (**Figure 5A-C**) within the damaged areas.
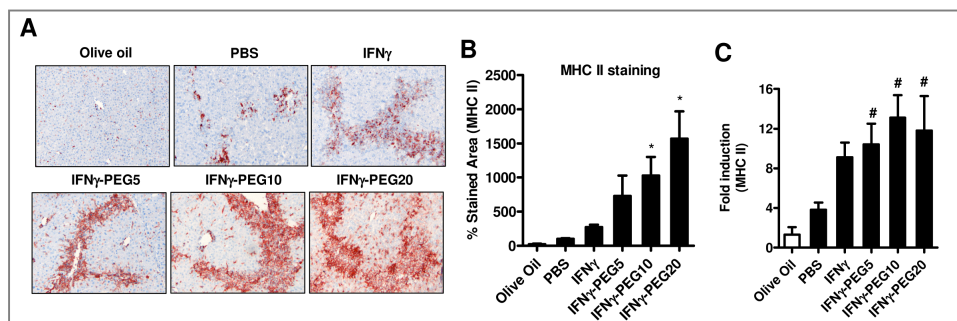
Figure 5: Increased MHC-II expression with PEGylated IFNγ constructs *in vivo*. Representative photomicrographs **(A)** and quantitative analysis **(B)** and gene expression analysis **(C)** of MHC-II in liver samples. Animals were treated with either olive oil (treated with PBS as control) or CCl$_4$ plus PBS, IFNγ or different PEGylated-IFNγ constructs. Scale bars; 100μm.

3.5. Attenuation of liver fibrosis with PEGylated IFNγ conjugates

IFNγ and different PEGylated IFNγ constructs were subsequently examined for their anti-fibrotic effects in a CCl$_4$-induced acute liver fibrosis model in mice. After two intravenous injections, PEGylated IFNγ constructs induced a strong inhibition in collagen I expression accompanied by substantial reduction in α-SMA- and desmin-positive hepatic stellate cells (**Figure 6A-C**). The reductions of fibrotic parameters observed in stainings were paralleled by reductions in the respective transcript levels as assessed by quantitative rtPCR (**Figure 7**). The anti-fibrotic effects with IFNγ-PEG were significantly enhanced with increasing PEG size. In contrast, treatment with IFNγ did not induce a significant reduction of any of these parameters, which is most likely due to the short half-life of IFNγ.
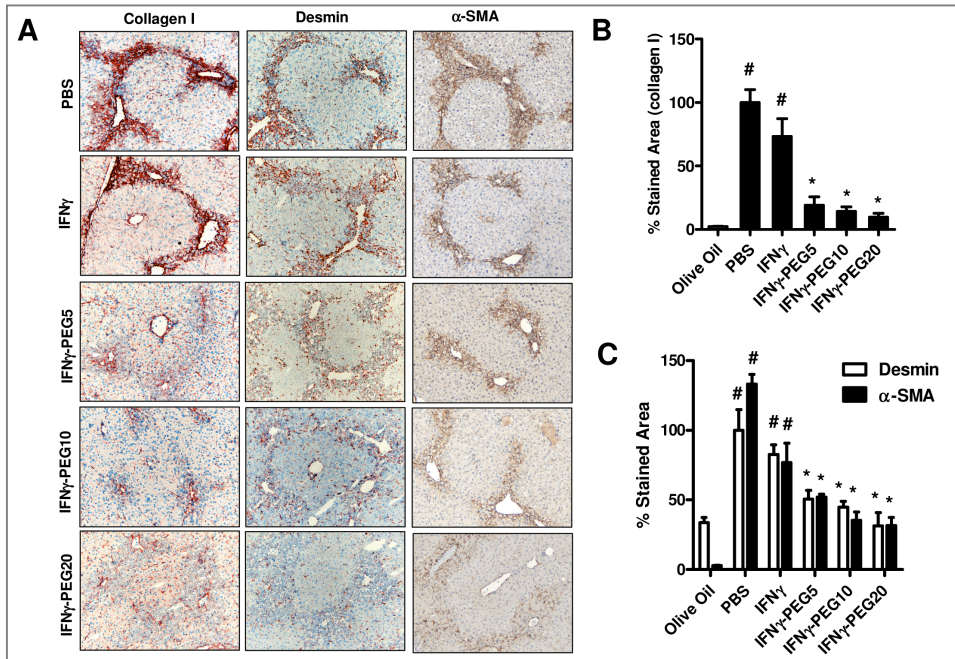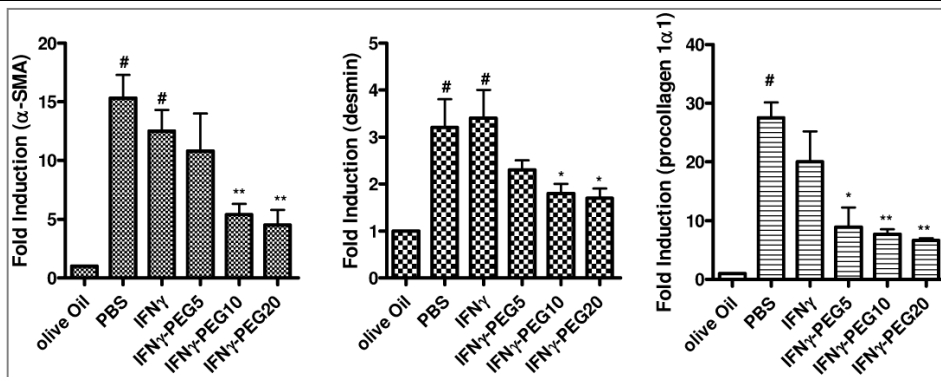
Figure 6: Reduction in fibrotic parameters induced by PEGylated IFNγ *in vivo*. Representative photomicrographs **(A)** and quantitative analysis of collagen I **(B),** αSMA and desmin **(C)** positive liver sections from olive oil (CCl₄ vehicle as a control) and fibrotic animals treated with PBS, IFNγ and different PEGylated-IFNγ constructs. Scale bars; 100μm. Bars represent mean ± SEM of 4 mice per group. #$p<0.05$ versus olive oil and *$p<0.05$, **$p<0.01$ versus PBS treated-CCl₄ mice.

4. DISCUSSION

IFNγ is a pro-inflammatory cytokine and has been studied pre-clinically for the treatment of immunological, viral and cancer diseases due to its pleiotropic activities [28]. It has also been explored as a potential treatment for renal, idiopathic and liver fibrosis [13,29,30]. Despite the various therapeutic effects of IFNγ, its clinical use is limited to only a few diseases, due to rapid clearance from the body. Some attempts have been made to prolong the half-life or to enhance activity of IFNγ by incorporating it into hydrogels, nanoparticles, liposomes, microspheres and elastomers [31,32], but none of them have reached to clinic. PEGylation of IFNα (PEGASYS and PEGIntron) has been clinically successful but this approach has strikingly not been applied for IFNγ.

In the present study, we PEGylated IFNγ with different sized linear PEG chains of 5KDa, 10KDa and 20KDa to find optimum PEGylation combined with unhindered receptor interaction. Following synthesis of PEGylated IFNγ constructs, we first evaluated their bio-distribution profiles and effects *in vitro.* Chemical modification can lead to reduced activity of IFNγ as reported by other studies [33,34], caused by a change in conformation or steric hindrance influencing receptor binding. Though PEGylated constructs showed a reduced biological activity compared to IFNγ in the absence of LPS but did not show significant differences in their biological activities in presence of LPS. In addition, PEGylated IFNγ

Figure 7: Reduction in mRNA expression levels of crucial fibrotic parameters (α-SMA, Desmin and procollagen 1α1) induced by PEGylated IFNγ *in vivo*. Effects of different constructs on the gene expression on crucial fibrotic parameters: α-SMA, Desmin and procollagen 1α1 in CCl4-induced liver fibrosis in mice. Animals were treated with either olive oil (CCl4 vehicle as a control) or CCl4 plus PBS, IFNγ or different PEGylated-IFNγ constructs. Bars represent mean ± SEM of 4 mice per group. #$p<0.05$ versus olive oil and *$p<0.05$, **$p<0.01$ versus PBS treated-CCl4 mice.

induced IFNγR signaling similar to native IFNγ as demonstrated with a reporter plasmid assay. Furthermore, these constructs showed even stronger effects than unmodified-IFNγ *in vitro* by inhibiting fibroblasts activation and collagen production in these cells. This increased effectivity *in vitro* indicates increased stability of IFNγ in biological environments due to the PEGylation.

We observed high up-regulation of IFNγ receptor expression during liver fibrosis (both in mice and human) and then we explored the uptake of radiolabeled IFNγ in fibrotic livers. We found a significant increase of IFNγ uptake in fibrotic livers compared to normal livers, but the plasma disappearance rate of IFNγ was still quite high. Therefore, we assumed that longer circulation of IFNγ due to PEGylation might result in even higher liver accumulation and thereby enhanced anti-fibrotic effects. We therefore explored the effects of PEGylation of IFNγ in CCl4-induced acute liver fibrosis model in mice.

Using radioactive studies, we demonstrated that PEGylated IFNγ constructs had a better pharmacokinetic profile compared to IFNγ *in vivo*. PEGylation of IFNγ increased the plasma circulation time, enhanced liver levels and reduced renal accumulation of IFNγ constructs compared to free IFNγ. Only IFNγ-PEG20 displayed lower liver accumulation, which, most likely, is due to its larger size that caused its longer circulation, and less accumulation into the collagen-rich fibrotic liver. In addition, PEGylated IFNγ constructs induced the up-regulation of MHC-II expression, a well-known activity of IFNγ [27]. The increase in MHC-II expression was consistent with increased size of PEGylation of IFNγ, while unmodified IFNγ induced moderate MHC-II expression, most likely due to rapid renal clearance.

Since PEGylation significantly improved the pharmacokinetics of IFNγ, we furthermore investigated PEGylated constructs for their therapeutic effectivity. All the IFNγ-PEG constructs induced significantly stronger anti-fibrotic effects *in vivo* compared to

IFNγ at the similar doses in the acute CCl₄-induced liver injury model in mice. The reduction of extracellular matrix deposition was accompanied with reduced activation and proliferation of hepatic stellate cells, a key pathogenic cell involved in the progression of liver fibrosis. While native IFNγ had only some effects, PEGylation of IFNγ led to the profound reductions in all the fibrotic parameters examined. The increased efficacy was already significant with IFNγ-PEG5 but was further potentiated with increased PEG size.

In the present study, the pharmacokinetic profile, *in vitro* and *in vivo* efficacies of the PEGylated IFNγ were critically evaluated. We have clearly demonstrated that PEGylation of IFNγ significantly improved its pharmacokinetic profile and therapeutic effectivity. Since the use of this potent cytokine for therapeutic purposes offers great opportunities, therefore further studies are warranted to explore further modifications of IFNγ. These long-circulating IFNγ constructs with a concomitant enhancement of the anti-fibrotic activity represent a step forward towards an effective anti-fibrotic therapy.

ACKNOWLEDGEMENTS

REFERENCES

(1) R. Bataller, D.A. Brenner, Liver fibrosis, J Clin Invest. 115 (2005) 209-218.

(2) D. Schuppan, N.H. Afdhal, Liver cirrhosis, Lancet. 371 (2008) 838-851.

(3) S.L. Friedman, Stellate cells: a moving target in hepatic fibrogenesis, Hepatology. 40 (2004) 1041-1043.

(4) S.L. Friedman, Hepatic stellate cells: protean, multifunctional, and enigmatic cells of the liver, Physiol Rev. 88 (2008) 125-172.

(5) O.A. Gressner, R. Weiskirchen, A.M. Gressner, Evolving concepts of liver fibrogenesis provide new diagnostic and therapeutic options, Comp Hepatol. 6 (2007) 7.

(6) D.C. Rockey, Current and future anti-fibrotic therapies for chronic liver disease, Clin Liver Dis. 12 (2008) 939-62, xi.

(7) E.M. Bonnem, R.K. Oldham, Gamma-interferon: physiology and speculation on its role in medicine, J Biol Response Mod. 6 (1987) 275-301.

(8) C.H. Miller, S.G. Maher, H.A. Young, Clinical Use of Interferon-gamma, Ann N Y Acad Sci. 1182 (2009) 69-79.

(9) K. Schroder, P.J. Hertzog, T. Ravasi, D.A. Hume, Interferon-gamma: an overview of signals, mechanisms and functions, J Leukoc Biol. 75 (2004) 163-189.

(10) P.J. Pockros, L. Jeffers, N. Afdhal, Z.D. Goodman, D. Nelson, R.G. Gish, K.R. Reddy, R. Reindollar, M. Rodriguez-Torres, S. Sullivan, L.M. Blatt, S. Faris-Young, Final results of a double-blind, placebo-controlled trial of the antifibrotic efficacy of interferon-gamma1b in chronic hepatitis C patients with advanced fibrosis or cirrhosis, Hepatology. 45 (2007) 569-578.

(11)   I. Rutenfranz, H. Kirchner, Pharmacokinetics of recombinant murine interferon-gamma in mice, J Interferon Res. 8 (1988) 573-580.

(12)   H.M. Younes, B.G. Amsden, Interferon-gamma therapy: evaluation of routes of administration and delivery systems, J Pharm Sci. 91 (2002) 2-17.

(13)   G.S. Baroni, L. D'Ambrosio, P. Curto, A. Casini, R. Mancini, A.M. Jezequel, A. Benedetti, Interferon gamma decreases hepatic stellate cell activation and extracellular matrix deposition in rat liver fibrosis, Hepatology. 23 (1996) 1189-1199.

(14)   W.I. Jeong, O. Park, S. Radaeva, B. Gao, STAT1 inhibits liver fibrosis in mice by inhibiting stellate cell proliferation and stimulating NK cell cytotoxicity, Hepatology. 44 (2006) 1441-1451.

(15)   M. Hamidi, A. Zarrin, M. Foroozesh, Novel delivery systems for interferons, Crit Rev Biotechnol. 27 (2007) 111-127.

(16)   G.E. Francis, D. Fisher, C. Delgado, F. Malik, A. Gardiner, D. Neale, PEGylation of cytokines and other therapeutic proteins and peptides: the importance of biological optimisation of coupling techniques, Int J Hematol. 68 (1998) 1-18.

(17)   S. Jevsevar, M. Kunstelj, V.G. Porekar, PEGylation of therapeutic proteins, Biotechnol J. 5 (2010) 113-128.

(18)   J.S. Kang, P.P. Deluca, K.C. Lee, Emerging PEGylated drugs, Expert Opin Emerg Drugs. 14 (2009) 363-380.

(19)   F.M. Veronese, G. Pasut, PEGylation, successful approach to drug delivery, Drug Discov Today. 10 (2005) 1451-1458.

(20)   T. Poynard, J. McHutchison, M. Manns, C. Trepo, K. Lindsay, Z. Goodman, M.H. Ling, J. Albrecht, Impact of pegylated interferon alfa-2b and ribavirin on liver fibrosis in patients with chronic hepatitis C, Gastroenterology. 122 (2002) 1303-1313.

(21)   C. Camma, B.D. Di, F. Schepis, E.J. Heathcote, S. Zeuzem, P.J. Pockros, P. Marcellin, L. Balart, A. Alberti, A. Craxi, Effect of peginterferon alfa-2a on liver histology in chronic hepatitis C: a meta-analysis of individual patient data, Hepatology. 39 (2004) 333-342.

(22)   Y.M. Kim, K. Son, A nitric oxide production bioassay for interferon-gamma, J Immunol Methods. 198 (1996) 203-209.

(23)   M.M. van Beuge, J. Prakash, M. Lacombe, E. Post, C. Reker-Smit, L. Beljaars, K. Poelstra, Increased Liver Uptake and Reduced Hepatic Stellate Cell Activation with a Cell-Specific Conjugate of the Rho-kinase Inhibitor Y27632, Pharm Res. (2011) .

(24)   J. Wu, P.A. Norton, Animal models of liver fibrosis, Scand J Gastroenterol. 31 (1996) 1137-1143.

(25)   A.H. van Boxel-Dezaire, G.R. Stark, Cell type-specific signaling in response to interferon-gamma, Curr Top Microbiol Immunol. 316:119-54. (2007) 119-154.

(26)   C.M. Horvath, The Jak-STAT pathway stimulated by interferon gamma, Sci STKE. 2004 (2004) tr8.

(27)   A. Muhlethaler-Mottet, B.W. Di, L.A. Otten, B. Mach, Activation of the MHC class II transactivator CIITA by interferon-gamma requires cooperative interaction between Stat1 and USF-1, Immunity. 8 (1998) 157-166.

(28)   M.A. Farrar, R.D. Schreiber, The molecular cell biology of interferon-gamma and its receptor, Annu Rev Immunol. 11 (1993) 571-611.

(29)   D. Bouros, K.M. Antoniou, A. Tzouvelekis, N.M. Siafakas, Interferon-gamma 1b for the treatment of idiopathic pulmonary fibrosis, Expert Opin Biol Ther. 6 (2006) 1051-1060.

(30)   S.D. Oldroyd, G.L. Thomas, G. Gabbiani, A.M. El Nahas, Interferon-gamma inhibits experimental renal fibrosis, Kidney Int. 56 (1999) 2116-2127.

(31)   J.L. Cleland, A.J. Jones, Stable formulations of recombinant human growth hormone and interferon-gamma for microencapsulation in biodegradable microspheres, Pharm Res. 13 (1996) 1464-1475.

(32)   F. Gu, H.M. Younes, A.O. El-Kadi, R.J. Neufeld, B.G. Amsden, Sustained interferon-gamma delivery from a photocrosslinked biodegradable elastomer, J Control Release. 102 (2005) 607-617.

(33)   B.M. Brooks, B.F. Flanagan, A.L. Thomas, J.W. Coleman, Penicillin conjugates to interferon-gamma and reduces its activity: a novel drug-cytokine interaction, Biochem Biophys Res Commun. 288 (2001) 1175-1181.

(34)   B.M. Brooks, A.L. Thomas, J.W. Coleman, Benzylpenicillin differentially conjugates to IFN-gamma, TNF-alpha, IL-1beta, IL-4 and IL-13 but selectively reduces IFN-gamma activity, Clin Exp Immunol. 131 (2003) 268-274.

SUPPLEMENTARY INFORMATION 1:

Supplementary Table 1: Sequence of the primers used for quantitative real-time PCR

Gene	Forward	Reverse
Human		
18s rRNA	CGGCTACCCACATCCAAGGA	CCAATTACAGGGCCTCGAAA
IFNγR1	CCAGCAACAGTTCCAGGCAT	CCGGGACCACGTCAGGAATA
Mouse		
Procollagen 1α1	TGACTGGAAGAGCGGAGAGT	ATCCATCGGTCATGCTCTCT
Desmin	ATGCAGCCACTCTAGCTCGT	CTCATACTGAGCCCGGATGT
GAPDH	ACAGTCCATGCCATCACTGC	GATCCACGACGGACACATTG
IFNγR1	GTAACCAGTCAGGCCCTTGT	CAACATGTGCGGTTTGTCAT
α-sma	ACTACTGCCGAGCGTGAGAT	CCAATGAAAGATGGCTGGAA

Abbreviations: 18s rRNA, 18s ribosomal RNA; IFNγR1, Interferon gamma receptor 1; GAPDH, Glyceraldehyde 3-phosphate dehydrogenase; MHC-II, major histocompatibility complex Class II; α-sma, alpha-smooth muscle actin.

Supplementary Table 2: Antibodies used for the immunostainings

| Antibody	Source	Dilution
Primary antibodies		
Monoclonal Mouse anti-α-SMA	Sigma	1:600
Polyclonal Goat anti-collagen I	Southern Biotech	1:100
Polyclonal Goat anti-collagen III	Southern Biotech	1:100
Polyclonal Goat anti-desmin	Santa Cruz	1:100
Monoclonal Rabbit anti-IFNγR1	Abcam	1:50
Secondary antibodies		
HRP-conjugated Rabbit anti-Goat	DAKO	1:100
HRP-conjugated Goat anti-rabbit	DAKO	1:100

Supplementary Table 3:
Analysis of band intensity to determine % of PEGylated IFNγ and free unconjugated IFNγ after chemical conjugation reactions evaluated from Western blot analysis using ImageJ software:

Compounds	PEG conjugated IFNγ	Free IFNγ monomer
IFNγ	-	100 %
IFNγ-PEG5	94.9 %	5.1%
IFNγ-PEG10	91.9%	8.1%
IFNγ-PEG20	90.0%	10.0 %

Supplementary Table 4:

Liver accumulation of IFNγ in normal vs acute liver injury mouse model:

| Liver	AUC (h*%dose)
IFNγ (normal mice)	39.19
IFNγ (CCl$_4$-treated mice)	64.06
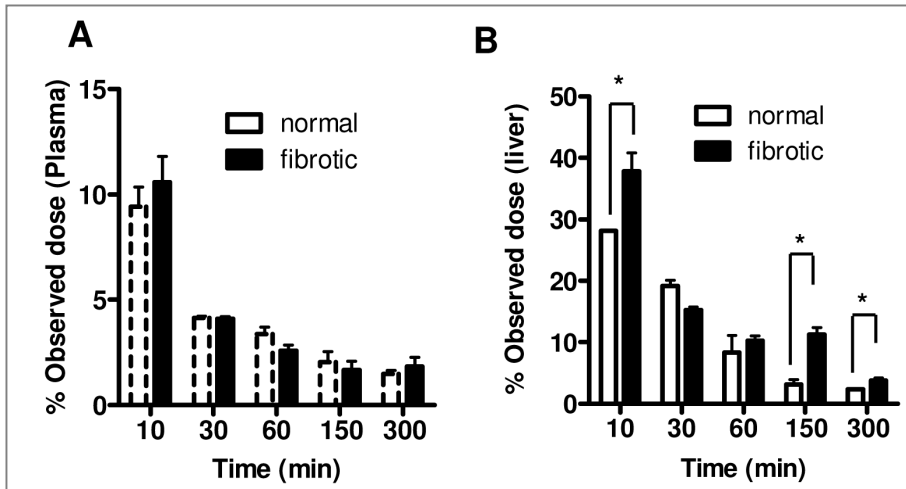
Supplementary Figure 1: Biodistribution of ^{125}I-IFNγ in normal and fibrotic mice. Plasma levels **(A)** and liver levels **(B)** of radiolabeled IFNγ in mice with CCl$_4$-induced liver fibrosis versus normal mice at different time intervals. *denotes significance of $p<0.05$.

SUPPLEMENTARY INFORMATION 2:

Adverse Effects of PEGylated IFNγ in acute CCl₄-induced liver injury model in mice:

Interferon gamma is a pro-inflammatory cytokine and prolonged circulation of IFNγ might initiate increased inflammatory responses. We therefore studied the infiltration and activation of inflammatory cells in livers and other organs. We found that PEGylation of IFNγ with larger PEG moieties induced more extensive intra-hepatic infiltration of neutrophils and F4/80 positive macrophages (**Supplementary Figure. 2A and 2B**).
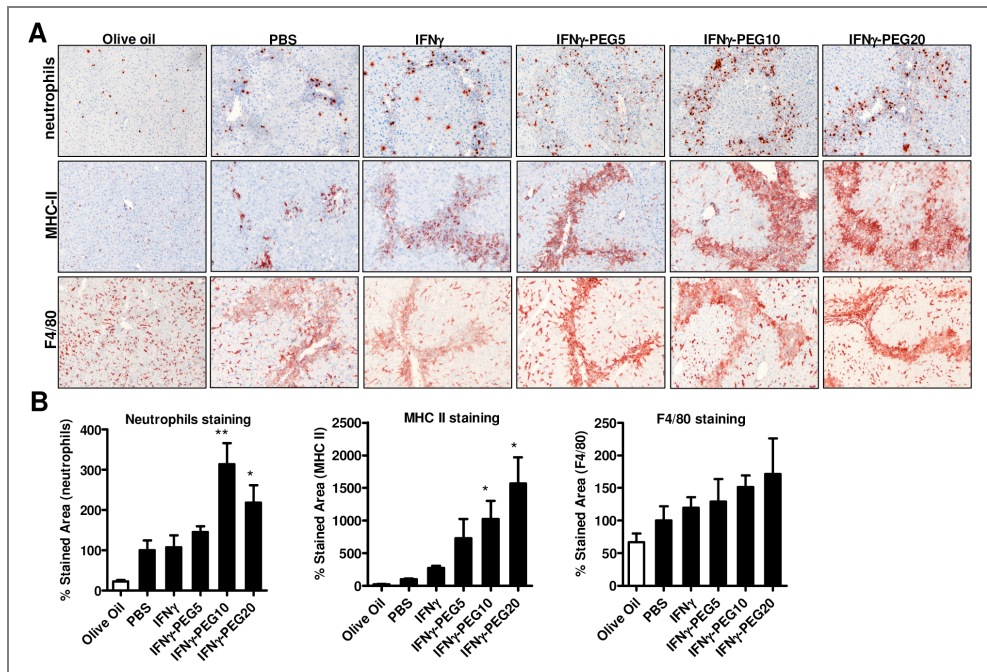
Supplementary Figure 2: PEGylated IFNγ induced macrophage activation and infiltration of macrophages and neutrophils in fibrotic livers. (A) Representative pictures and **(B)** Quantitative analysis of liver sections stained for neutrophils, macrophages and MHC-II. Scale bars; 100μm. Bars represent mean ± SEM of 4 mice per group. *p<0.05 and **p<0.01 vs. PBS treated-CCl₄ group.

Furthermore, longer circulating PEGylated IFNγ led to increased macrophage activation as confirmed by major histocompatibility complex (MHC-II) expression in livers and other organs such as kidney, heart and lungs (**Supplementary Figure 2 and 3A**). Moreover, administration of IFNγ-PEG molecules led to leucopenia, acute weight loss and increased plasma levels of inflammatory cytokines such as IL-6 and TNFα (**Supplementary Figure 3B-E**). Of note, the degrees of these pro-inflammatory effects were paralleled with the increase in the size of PEG moieties.
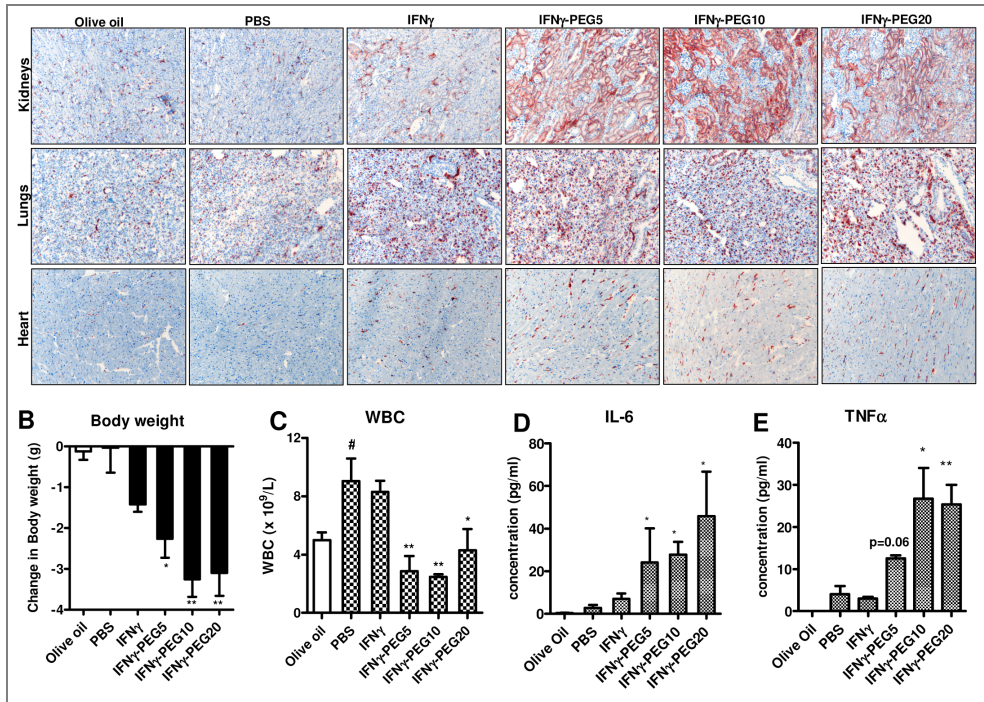
Supplementary Figure 3: Increased systemic inflammation after administration of PEGylated IFNγ conjugates. (A) Representative photos showing MHC-II expression in kidneys, lungs and heart from PBS-treated olive oil and PBS, IFNγ or PEGylated-IFNγ treated fibrotic animals. Scale bars; 100μm. **(B)** Change in body weight of animals receiving different treatments. **(C)** White blood cell (WBC) count of PBS, IFNγ or PEGylated-IFNγ treated fibrotic and olive oil control animals. **(D and E)** TNF-α and IL-6 plasma levels in normal (olive oil open bars) and CCl_4-treated mice (closed bars) following IFNγ or IFNγ-constructs administration. #$p<0.05$ vs. olive oil mice and *$p<0.05$ and **$p<0.01$ vs. PBS-treated CCl_4 mice.